Available online at www.sciencedirect.com

ScienceDirect

journal homepage: http://www.elsevier.com/locate/acme

Original Research Article

# Development of a simple bond-slip model for joints monitored with the DIC technique

*Hugo C. Biscaia* [a,*], *Noel Franco* [b], *Carlos Chastre* [c]

[a] *FSE, UNIDEMI, Department of Civil Engineering, Faculdade de Ciências e Tecnologia/Universidade Nova de Lisboa, 2829-516 Caparica, Portugal*

[b] *Department of Civil Engineering, Faculdade de Ciências e Tecnologia/Universidade Nova de Lisboa, 2829-516 Caparica, Portugal*

[c] *CERIS, ICIST, Department of Civil Engineering, Faculdade de Ciências e Tecnologia/Universidade Nova de Lisboa, 2829-516 Caparica, Portugal*

ARTICLE INFO

*Article history:*
Received 21 October 2017
Accepted 21 June 2018
Available online 29 July 2018

*Keywords:*
Bond-slip model
Bond
Interfaces
Closed-form solution
DIC technique

ABSTRACT

The monitoring of structures has undergone important advances with the improvements of digital cameras available on the market. Thus, the Digital Image Correlation (DIC) technique has become a viable way of studying engineering problems. Recently it has been used in the debonding failure process between the reinforcement and the substrate. The methods or methodologies that should be followed to obtain the results associated to the debonding phenomenon using the DIC technique need to be better understood and studies on this topic are scarce. The present work therefore proposes a new and inexpensive method to monitor the interfacial behaviour between a reinforcement material and a substrate by combining the use of the DIC technique and a simplified nonlinear bond-slip model. For the validation of the proposed method, a series of single-lap shear tests with a sufficient long bond length carried out by the authors are used. Based on the slip distribution obtained from the DIC technique, it was found that a third-degree polynomial function can be used to approximate the interfacial bond-slip curve of the joint. The validation of the model is made with several analytical solutions using the proposed bond-slip model.



## 1. Introduction

Nowadays, the monitoring of structures has improved considerably, namely in the reading displacements or strains by taking several pictures of the same area, previously painted with a randomly speckled pattern. The combination of high performance digital cameras with algorithms that are able to identify and consequently follow small displacements of a finite area has been utilized recently by researchers, e.g. [1–9]. The costs associated to the use of the Digital Image Correlation (DIC) technique for the monitoring of a structure are much lower than other conventional techniques such as strain gauges or Linear Variable Displacement Transducers (LVDT), etc., because free algorithms and software can be easily found

* *Corresponding author.*
E-mail addresses: hb@fct.unl.pt (H.C. Biscaia), ni.franco@campus.fct.unl.pt (N. Franco), chastre@fct.unl.pt (C. Chastre).

https://doi.org/10.1016/j.acme.2018.06.009
1644-9665/

on the web [10–12] that reduces the costs. Unlike strain gauges or LVDTs that measure a single point, the DIC technique allows several points (an area) at each measurement [2,3,8] to be monitored.

This technique has been used recently [1,4–7] to monitor the debonding of a reinforcement material from the substrate. However, due mainly to the very small displacements (usually less than 1 mm) associated to the debonding process of a reinforcement from the substrate, the displacement or relative displacement (or slip) fields are difficult to obtain especially at the beginning of the debonding process, where the slips are tiny (~0.01 mm). For the correct interpretation of the debonding process, some researchers [1,4,6] have avoided techniques based exclusively on the DIC technique since the field of displacements has several ''peaks and valleys''. These discontinuities compromise the calculation of the strains or bond stresses developed within the interface because it is deeply affected when the first and second derivatives with respect to the *x*-axis (along the bonded length) are determined.

To bypass these difficulties, some researchers [1,4,6] have used approximate solutions of the slip distributions derived from other researchers [13]. This procedure presupposes that the local bond-slip relationship should be previously known, which in the case of, e.g., Fiber Reinforced Polymers (FRP) externally bonded to a concrete substrate has been experimentally determined from single [14–17] or double-lap shear tests [16,18] or even from flexural tests [16,19]. Based on these experimentally determined bond-slip relationships, several authors have proposed different numerical strategies based on the Finite Difference Method [20,21], Finite Element Method [22,23], Distinct Element Method [24,25] or based on the discretization of the bonded joints with nonlinear springs [26,27] to simulate the debonding process between an FRP composite and a concrete substrate. Alternatively, analytical models have been developed [28–30] to define, through mathematical functions, the slip distribution within the interface throughout the debonding process. Consequently, these continuous mathematical functions have been used to smooth the slip results obtained from the DIC technique. Besides, its use also facilitates the determination of the strains and especially the bond stresses developed within the interface. So, such a strategy would allow the debonding process to be monitored until the failure of the joint, helping to ensure the correct interpretation, analysis and discussion of the results by way of a ''cheap'' monitoring solution.

The bonded joint between the stainless steel flat bar and the concrete substrate is an example of a bonded joint that has not been the subject of much analysis. In this case, there is no exact or approximate solution for the slip distributions, which prevents the use of the expressions available in the literature [13] which are based on an exponential bond-slip model. Still, the determination of the bond-slip curve using exclusively the DIC technique has deserved some attention in the literature [9] but there is scarce information covering the, e.g., stainless steel-to-concrete interfaces. In the present work an easy but accurate method to estimate the local bond-slip curve of a bonded joint using only the DIC technique is proposed. The calibration of the model is presented as well. Based on the slip distributions obtained from the DIC technique, a 3rd degree polynomial function was found to be able to represent the local bond-slip curve of the joint. Due to the limited information about the interfacial behaviour of stainless steel-to-concrete interfaces, the results are compared with six tests carried out in [9] which were considered there to have a sufficient bond length. Based on this model, a closed-form solution for the description of the debonding process is derived and the results are also compared and validated with those six tests which specimens had different bonded lengths that ranged between 240 and 800 mm.

The measurements of the displacements made in [9] with the DIC technique were carried out through the use of a digital camera that captured photos with 3456 × 5184 pixels at intervals of 5 s during the tests, and to avoid undesired shadows on the monitored surfaces, an artificial spotlight with 100 W was used. It is noteworthy to mention that the failure modes observed from the single-lap shear tests in [9] were mainly adhesive between the stainless steel and the adhesive, and, in a couple of specimens, a detachment of a very thin layer of concrete could be observed in some bonded regions of the stainless steel-to-concrete interface. Therefore, it is expected that no relevant out-of-plane displacements may develop in the tests which allow the use of the simple, but yet accurate, approach through the 2D DIC technique. The results showed good correlation with the tests and the formulations herein developed, due to its simplicity and wide use, it is suitable for adoption in an international code.

## 2. Formulation of the proposed bond-slip model

The determination of the bond-slip curve from the DIC technique is quite complex mainly due to the discontinuities obtained in the slip distribution, unlike when using strain gauges, which allow continuous slips distributions to be measured [6,9]. The use of strain gauges means that distance between them should be no longer than 50 mm [9] because the determination of the bond stresses with a constant distribution between consecutive strain gauges is adopted and the slips assume a parabolic distribution [30,31]. To avoid the discontinuities (noisy signal) obtained from the DIC results, a fitting curve should be applied to the slip distribution, which simplifies the assessment of the bond characterization of the bonded interface and consequently the determination of the bond-slip curve becomes easier to estimate. In the following subsections, the formulation of the proposed bond-slip model is presented.

### 2.1. *Theoretical background*

The proposed model is based on the approximation of the slip distribution obtained from the DIC technique at the start of debonding, whether the bonded joint is completely or partially monitored along the bond length. It should be noted that as the bond behaviour of the interface is initially unknown, an exact or approximate solution for the debonding phenomenon is initially unknown as well. Thus, since the solutions for the debonding of the FRP-to-concrete interface are known [13,32,33], the discussions for other bonded joints such as FRP-to-timber/steel or stainless steel-to-concrete interfaces are still open and therefore, such particular solutions were not

considered here. Nevertheless, the proposed bond-slip model may be also seen as a simplification of the exponential bond-slip model often used to characterize the interfacial behaviour of FRP-to-concrete interfaces and it could be applied, as already mentioned, to other bonded interfaces as well as this one.

During the debonding process, the slip distribution is characterized by a nonlinear distribution along the bonded length, with its highest value localized at the pulled end (@x = $L_b$) and the lowest at the free end (@x = 0). One concavity (face up) is also observed in the bonded length domain. Taking into consideration these aspects, the following function should be able to describe the slip distribution of the interface:

$$s(x) = \frac{a}{1 + e^{b(L_b - x)}} \tag{1}$$

where $a$ and $b$ are constants to be determined from fitting the curve to the experimental results obtained from the DIC technique and $L_b$ is the bond length. As mentioned, this function depends on the definition of two parameters, one being half of $a$ corresponding to the slip at the pulled end and $b$ is responsible for the shape of the function, which becomes more accentuated with the increase of $b$. Parameter $b$ should be higher than zero and is, in this case, a straight-line parallel to the $x$-axis at a distance of $a/2$. Fig. 1 shows how these parameters affect Eq. (1).

For the definition of the proposed bond-slip model, Eq. (1) is used and subsequent strain-slip analysis or stress transfer between bonded materials will be derived next and will be the focus of a deep analysis in the subsequent subsections. It should be mentioned that the proposed model should be limited to those cases where the bond length is sufficiently long enough and when the substrate is considered stiff enough that the strains in it can be ignored.

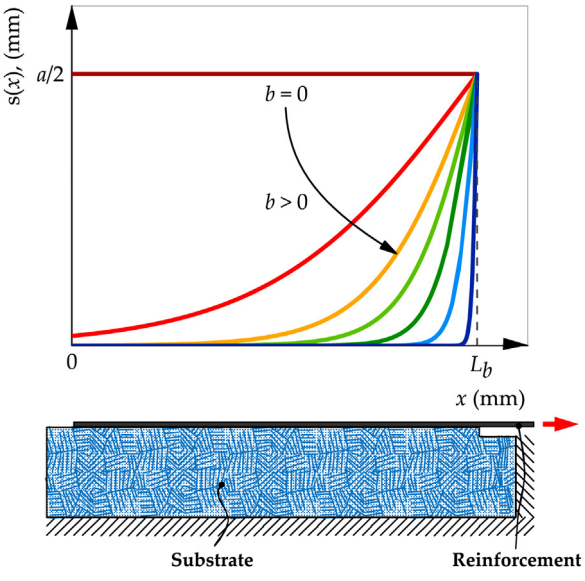


**Fig. 1 – Proposed function for the definition of the slip distributions, s(x), of a bonded interface.**

### 2.2. *The bond-slip model*

To obtain the bond-slip model, it is first necessary to define the derivative of Eq. (1) with respect to x:

$$\frac{ds}{dx} = \frac{a \cdot b \cdot e^{b(L_b - x)}}{\left(1 + e^{b(L_b - x)}\right)^2}. \tag{2}$$

The slips are the relative displacements between the surface of the reinforcement ($u_r$) and the surface of the substrate ($u_s$):

$$s = u_r - u_s. \tag{3}$$

The first derivative of Eq. (3) with respect to x leads to:

$$\frac{ds}{dx} = \frac{du_r}{dx} - \frac{du_s}{dx} \tag{4}$$

where $du_r/dx$ and $du_s/dx$ are the strains in the reinforcement material and in the substrate, respectively. Comparing the strains developed in the reinforcement and in the substrate, the latter can be ignored and the strain distribution in the reinforcement can be determined by introducing Eq. (4) into Eq. (2), leading to:

$$\epsilon_r = \frac{du_r}{dx} = \frac{a \cdot b \cdot e^{b(L_b - x)}}{\left(1 + e^{b(L_b - x)}\right)^2}. \tag{5}$$

Regarding Eq. (1) once again, when the exponential term is isolated, leads to the following equality:

$$e^{b(L_b - x)} = \frac{a}{s} - 1 \tag{6}$$

which, introduced into Eq. (5), yields:

$$\epsilon_r = \frac{b}{a} \cdot s \cdot (a - s). \tag{7}$$

From Eq. (7), it can be noted that the strain-slip relationship is defined by a 2nd degree polynomial function with negative concavity (faced down). The maximum strain ($\epsilon_{r,max}$) and the ultimate slip of the bonded joint ($s_{ult}$) can be determined through the first derivative of Eq. (7), with respect to s, which, when equated to zero, gives:

$$\frac{d}{ds}\left[\frac{b}{a} \cdot s \cdot (a - s)\right] = 0 \rightarrow s_{ult} = \frac{a}{2}. \tag{8}$$

Hence, when the value of $s_{ult}$ is introduced into Eq. (7), the maximum strain in the reinforcement at its complete separation from the substrate has initiated, i.e. with no stress transfer between materials, and is obtained according to:

$$\epsilon_{r,max} = \frac{a \cdot b}{4} = \frac{s_{ult} \cdot b}{2} \tag{9}$$

The maximum strain developed in the reinforcement is an important aspect for the design of these bonded joints. Also, if Eq. (8) is introduced into Eq. (9), it can be seen that parameter $b$

depends on the ultimate slip and on the maximum strain developed in the reinforcement at its pulled end:

$$b = \frac{2 \cdot \epsilon_{r,\max}}{s_{ult}}. \tag{10}$$

Regarding Eq. (1) once again, the slip distribution at the start of debonding can be rewritten as:

$$s(x) = \frac{2s_{ult}}{1 + e^{\frac{2\epsilon_{r,\max}}{s_{ult}}(L_b - x)}}. \tag{11}$$

Considering a finite segment $dx$ of the bond length, the following equilibrium equation can be established, e.g. [31–36]:

$$\frac{d\sigma_r}{dx} - \frac{\tau(x)}{t_r} = 0 \tag{12}$$

where $t_r$ is the thickness of the reinforcement. Assuming the elastic behaviour of the reinforcement, its first derivative with respect to $x$ leads to:

$$\frac{d\sigma_r}{dx} = E_r \cdot \frac{d\epsilon}{dx} \tag{13}$$

which introduced in Eq. (12) yields:

$$\tau(x) = E_r \cdot t_r \cdot \frac{d\epsilon}{dx} \tag{14}$$

where $E_r$ is the elastic modulus of the reinforcement. The determination of the local bond-slip curve of the joint can be found by rewriting Eq. (14) as:

$$\tau(x) = E_r \cdot t_r \cdot \frac{d\epsilon}{ds} \cdot \frac{ds}{dx} \tag{15}$$

and introducing Eq. (2) and the first derivative of Eq. (7) with respect to $s$ into Eq. (15) yields:

$$\tau(s) = \left(\frac{b}{a}\right)^2 \cdot 2s \cdot (s - a)\left(s - \frac{a}{2}\right) \cdot E_r \cdot t_r. \tag{16}$$

Therefore, Eq. (16) corresponds to the bond-slip curve developed within the reinforcement and the concrete interface and it is defined by a 3rd degree polynomial function. The lower limit of the bond-slip curve corresponds to zero slip with zero bond stress, whereas the upper limit is defined by the ultimate slip ($s_{ult}$), which also corresponds to zero bond stress. The maximum bond stress ($\tau_{max}$) of the interface is defined with the help of the first derivative of Eq. (16) with respect to $s$, which, when equated to zero, the maximum slip ($s_{max}$) of the interface, i.e. the slip corresponding to the maximum bond stress, is obtained:

$$s_{max} = \frac{3 - \sqrt{3}}{6} \cdot a \tag{17}$$

and when introduced into Eq. (16) gives:

$$\tau_{max} = \frac{\sqrt{3}}{18} \cdot a \cdot b^2 \cdot E_r \cdot t_r. \tag{18}$$

It should be noted that the bond stress transfer at the debonding initiation can also be obtained, but to do this it is necessary to introduce the first derivative of Eq. (5) with respect to $x$ into Eq. (14), which gives:

$$\tau(x) = E_r \cdot t_r \cdot \frac{a \cdot b^2 \cdot e^{b(L_b - x)} \cdot \left(e^{b(L_b - x)} - 1\right)}{\left(1 + e^{b(L_b - x)}\right)^3}. \tag{19}$$

### 2.3. Fracture energy

Another parameter often used to predict the strength of a bonded joint is the fracture energy released during the debonding process of the joint, which is defined as [22]:

$$G_F = \int_0^{s_{ult}} \tau(s) ds \tag{20}$$

where $\tau(s)$ is the interfacial bond-slip relationship already defined in Eq. (16). Thus, introducing Eq. (16) into Eq. (20) and integrating it, gives:

$$G_F = \frac{(a \cdot b)^2}{32} \cdot E_r \cdot t_r. \tag{21}$$

### 2.4. Estimation of the effective bond length

Another important aspect on the debonding phenomenon is the length beyond which the load (or strain) cannot increase any further. In this sense, a good estimation of the effective bond length ($L_{eff}$) is crucial for the maximization of the interface strength. Thus, based on the proposed model, an easy way to estimate this parameter can be established by assuming that a slip lower than 0.005 mm is sufficiently small enough to develop negligible bond stresses. Thus, from Eq. (1) and considering $L_{eff} = L_b - x$, the effective bond length can be estimated according to:

$$L_{eff} = \frac{1}{b} \cdot \ln(200a - 1) \tag{22}$$

The effective bond length is also defined by only two parameters that can be easily determined, as will be demonstrated in Section 3, from a method based on the slip distribution obtained from the DIC technique.

## 3. Calibration of the bond-slip model

For the calibration of the local bond-slip model it is important to adopt the correct methodology to define parameters $a$ and $b$ with precision. One method is based on the slip distribution at the start of debonding. In order to facilitate the explanations on how this method should be used, the tests carried out in [9] will be considered. These results consist of a series of single-lap shear tests with stainless steel flat strips ($E_r$ = 192 GPa) with a cross section of 5 mm × 20 mm (thickness × width) externally bonded to a concrete substrate with an average

maximum compression stress of 24.1 MPa. For the bonding, epoxy resin S&P 220 was used, which, according to the supplier, has a compression strength higher than 70 MPa, a shear strength higher than 26 MPa and a Young modulus higher than 7.1 GPa. The single-lap shear tests were carried out under a monotonic load with a constant velocity of 4 kN/min until complete debonding. Since the proposed method should be applied only to those cases where the bonded lengths are higher than the effective bond length, only the samples meeting these conditions will be used and presented. Therefore, the calibration of the local bond-slip model will be set for the samples with bonded lengths greater than 235 mm, which corresponds to six specimens with bonded lengths of 240, 300, 400, 560, 640 and 800 mm.

Fig. 2 shows the steps that must be followed in order to obtain the interfacial behaviour of the bonded joint: (a) identify the ultimate slip of the bonded joint through the velocity of the test ($ds/dt$) plus the slip at the pulled end vs. time curve; (b) minimize the error between experimental and the theoretical slip distribution stated in (1); and (c) define the local bond-slip curve of the joint. Thus, from the measurements provided by the DIC technique during the test, the first derivate of the slip with respect to time should be sufficient to identify the instant when the test started to speed up. When this happened it meant that the reinforcement began to separate from the substrate and thus, the ultimate slip of the joint had been reached at that exact instant. From the slip at the pulled end vs. time curve, it is now possible to identify with precision the value of the ultimate slip. It should be noted that to achieve this, it is important to perform the test with a load control because otherwise, i.e. with a displacement control, the slip-time relationship will be defined by a straight line with a single slope that corresponds to the velocity adopted in the test. Under a load control, an initial curve will be seen and when the slips start to increase rapidly with time it means that the reinforcement began to separate completely from the substrate and that transition point will correspond to the ultimate slip. Then, the corresponding slip distribution obtained from the DIC technique at this time should be compared with Eq. (1) and parameters $a$ and $b$ should be defined. For the first parameter, $a$, Eq. (8) allows its calculation as a result of the identification of the ultimate slip in the previous step (see Fig. 1a), whereas parameter $b$ can be found by the lowest square minimization process between the slips obtained from the DIC technique ($s_x^{DIC}$) and from the analytical expression ($s_x^a$) stated in (1) according to:

$$\xi = \min_b \sum_0^x \left(s_x^a(b) - s_x^{DIC}\right)^2 \tag{23}$$

Therefore, the calibration of the proposed bond-slip curve is dependent on one single parameter $b$, which facilitates this minimization process. Regarding Eq. (10), the maximum strain developed in the reinforcement can be now predicted and all the subsequent information about the debonding process can be easily estimated. Thus, it should be noted that the debonding process of the joint is estimated without needing the use of strain gauges, pressure cells or data loggers for the acquisition of data and it is based exclusively on the measurements (slips) taken with the DIC technique instead.

To exemplify all the explanations provided previously, Fig. 3 shows the adjustments of Eq. (1) to the experimental data of the six specimens tested in [9]. The slips obtained from the DIC technique and shown in Fig. 3 were calculated according to Eq. (3), i.e. the displacements developed on the surface of the stainless steel and on the surface of the concrete in the vicinity of the stainless steel strip were measured [9]. The results show that Eq. (1) is able to represent well the slip distribution along the "peaks and valleys" obtained from the experiments. It should be noted that the bonded area covered by the DIC technique should fit into the effective bond length, which emphasizes the importance of having an initial idea of the value of the effective bond length. Still, as shown in Fig. 4, the specimen with a bonded length of 560 mm had an estimated bond-slip curve which was quite different from the remaining ones due to the slips obtained from the DIC technique at approximately $x = 370$ mm (see Fig. 3d) being relatively large when compared with its free end.

## 4. Closed-form solution for the debonding process

The debonding process of the joint can be studied once the governing equilibrium equation of the problem is established. Thus, from Eq. (12) and assuming the elastic regime of the reinforcement, the equilibrium condition of the bonded joint is [15,26,29,31–37]:

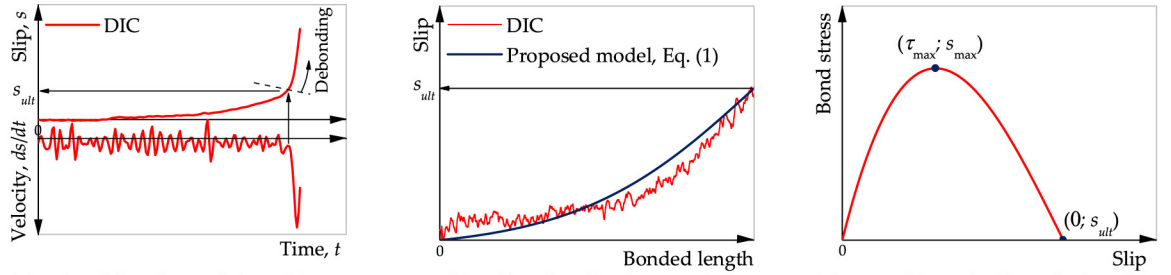


(a) Identification of the ultimate slip. (b) Slip distribution at the debonding initiation. (c) Local bond-slip relationship.

**Fig. 2 – Methodology for the calibration of the local bond-slip relationship.**

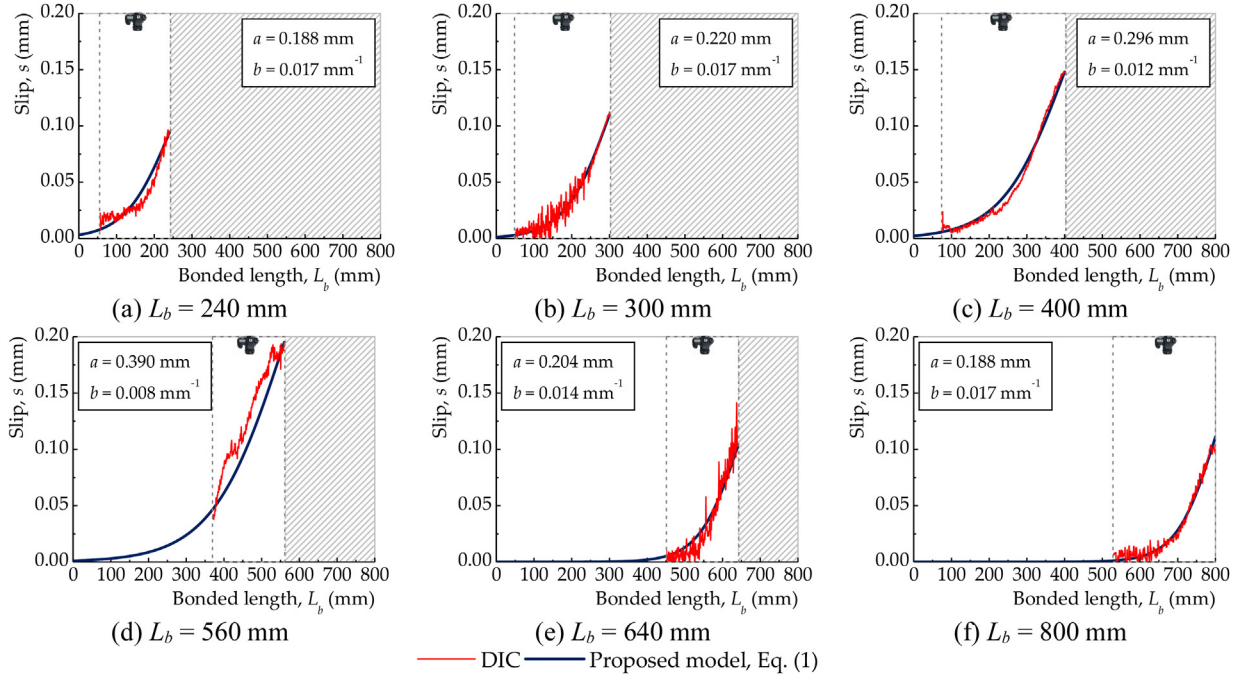


**Fig. 3 – Calibration of the slip distribution with the tests carried out in another study [9].**

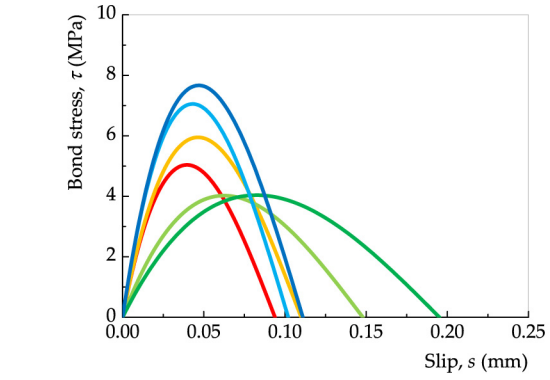


| Specimen [9] | $s_{max}$ (mm) | $s_{ult}$ (mm) | $\tau_{max}$ (MPa) | $\varepsilon_{r,max}$ (%) | $G_F$ (N/mm) |
|---|---|---|---|---|---|
| SS-EBR-L240 | 0.040 | 0.094 | 5.04 | 0.079 | 0.307 |
| SS-EBR-L300 | 0.047 | 0.110 | 5.95 | 0.093 | 0.425 |
| SS-EBR-L400 | 0.063 | 0.148 | 4.02 | 0.089 | 0.387 |
| SS-EBR-L560 | 0.083 | 0.195 | 4.04 | 0.076 | 0.512 |
| SS-EBR-L640 | 0.043 | 0.102 | 7.05 | 0.070 | 0.468 |
| SS-EBR-L800 | 0.047 | 0.111 | 7.67 | 0.078 | 0.553 |

**Fig. 4 – Definition of the local bond-slip relationships accordingly to the proposed model.**

$$\frac{d^2s}{dx^2} - \frac{\tau(s)}{E_r \cdot t_r} = 0 \tag{24}$$

and introducing Eq. (16) leads to:

$$\frac{d^2s(x)}{dx^2} = 2\left(\frac{b}{a}\right)^2 \cdot s \cdot (s-a)\left(s-\frac{a}{2}\right). \tag{25}$$

Considering that:

$$\frac{d^2s(x)}{dx^2} = \frac{d}{dx}\left(\frac{ds}{dx}\right) = \frac{d}{ds}\left(\frac{ds}{dx}\right)\frac{ds}{dx} = \frac{1}{2}\cdot\frac{d}{ds}\left(\frac{ds}{dx}\right)^2. \tag{26}$$

then, Eq. (3) can be rewritten as:

$$\left(\frac{ds}{dx}\right)^2 = 4\left(\frac{b}{a}\right)^2 \int 2s \cdot (s-a)\left(s-\frac{a}{2}\right)ds \tag{27}$$

which, when integrated, leads to:

$$\frac{ds}{dx} = \pm\sqrt{\left(\frac{b}{a}\right)^2 \cdot s^2(s-a)^2 + C_1} \tag{28}$$

where $C_1$ is a constant that is determined from the boundary conditions of the debonding problem @ $x = 0$:

$$\frac{ds}{dx}(x=0) = 0 \tag{29a}$$

and

$$s(x=0) = 0. \tag{29b}$$

Imposing the boundary conditions stated in (29a) and (29b), constant $C_1$ is zero. As will be seen next, only the negative solution in Eq. (28) is valid in the present case and it can be rewritten as:

$$\int \frac{ds}{s\cdot(s-a)} = -\frac{b}{a}\int dx \tag{30}$$

and when solved, it gives:

$$\frac{1}{a}\cdot\ln\left(\frac{a}{s}-1\right) + C_2 = -\frac{b}{a}\cdot x \tag{31}$$

where the term in the logarithmic function is always greater than zero and $C_2$ is a constant that can be determined from the boundary condition:

$$s(x=L_b) = s_{L_b} \tag{32}$$

where $s_{Lb}$ is the slip developed at $x = L_b$, i.e. at the pulled end and therefore:

$$C_2 = -\frac{b}{a}\cdot L_b - \frac{1}{a}\cdot\ln\left(\frac{a}{s_{L_b}}-1\right). \tag{33}$$

Introducing Eq. (33) into Eq. (31), the slips developed within the bonded joint are:

$$s(x) = \frac{a}{1+e^{b(L_b-x)}\cdot\left(\frac{a}{s_{L_b}}-1\right)} \tag{34}$$

where $s_{Lb}$ controls the simulation of the debonding process failure of the joint through a displacement loading history. Given this when the debonding process is initiated, then $s_{Lb} = s_{ult}$ and $a = 2s_{ult}$ (see Eq. (8)) and Eq. (34) becomes the same as Eq. (1), which validates the negative solution assumed earlier for Eq. (28). Thus, looking at Eq. (4) and recognizing that the strain in the substrate can be ignored, Eq. (28) can describe the strain distribution throughout the reinforcement as:

$$\epsilon_r(x) = \frac{a\cdot b\cdot s_{L_b}\cdot e^{b(L_b-x)}\cdot(a-s_{L_b})}{\left[e^{b(L_b-x)}\cdot(a-s_{L_b})+s_{L_b}\right]^2}. \tag{35}$$

The bond stresses developed within the interface are obtained through Eq. (14), which, from the first derivative of Eq. (4) with respect to x, leads to:

$$\frac{d^2s}{dx^2} = \frac{d\epsilon}{dx} \tag{36}$$

and taking into account Eq. (25), the bond stress distribution yields:

$$\tau(x) = E_r\cdot t_r\cdot a\cdot b^2\cdot s_{L_b}\cdot(s_{L_b}-a)\cdot\frac{e^{b(L_b-x)}\cdot\left(s_{L_b}-a\cdot e^{b(L_b-x)}+s_{L_b}\cdot e^{b(L_b-x)}\right)}{\left(s_{L_b}+a\cdot e^{b(L_b-x)}-s_{L_b}\cdot e^{b(L_b-x)}\right)^3}. \tag{37}$$

## 5. Validation of the bond-slip model

This section presents a series of results based on the closed-form solutions derived in Section 4 and compares them with the results obtained in the experimental program developed in [9]. Fig. 5 shows all the estimated bond-slip curves are compared with those obtained from the experimental work reported in [9] and Points i, ii, iii and iv were selected to represent the Elastic (Points i and ii) and the Softening stages (Points iii and iv) of the former bond-slip curves. Thus, Points i, ii, iii and iv correspond to four different slips at the pulled end as it will be illustrated in the subsequent subsections, i.e. at $s_{max}/2$, $s_{max}$, $(s_{max} + s_{ult})/2$ and $s_{ult}$, respectively.

### 5.1. *Strain-slip response*

Both experimental and theoretical relationships between the strains and the slips developed at the reinforcement pulled end are shown in Fig. 6 for each specimen tested in [9]. The results show that during the Elastic stage, the responses obtained from the proposed model agree very well with the experiments. However, in the specimen with $L_b = 300$ mm the analytical curve could not follow the tests as the failure of the specimens become closer and the maximum strains developed in the reinforcement were underestimated and overestimated, respectively. It should be noted also that the proposed model aims to predict the debonding failure process until the maximum strain is reached in the reinforcement. Still, after this point, the plateau at maximum strain can be obtained through the bond stress distribution defined in (37) and setting the equilibrium of the interface will lead to:

$$\epsilon_r = \frac{1}{E_r\cdot t_r}\int_0^{L_b}\tau(x)dx \tag{38}$$

where the integral is numerically solved by applying the trapezoidal rule. After this, and since the bond-slip model is limited by an ultimate slip, the strains in the reinforcement decrease until they reach zero with a corresponding slip equal to the ultimate value [32].

### 5.2. *Strain distribution*

The experimental strains developed in the stainless steel reinforcement and obtained from the strain gauges bonded along the stainless steel surfaces at specific Points i, ii, iii and iv

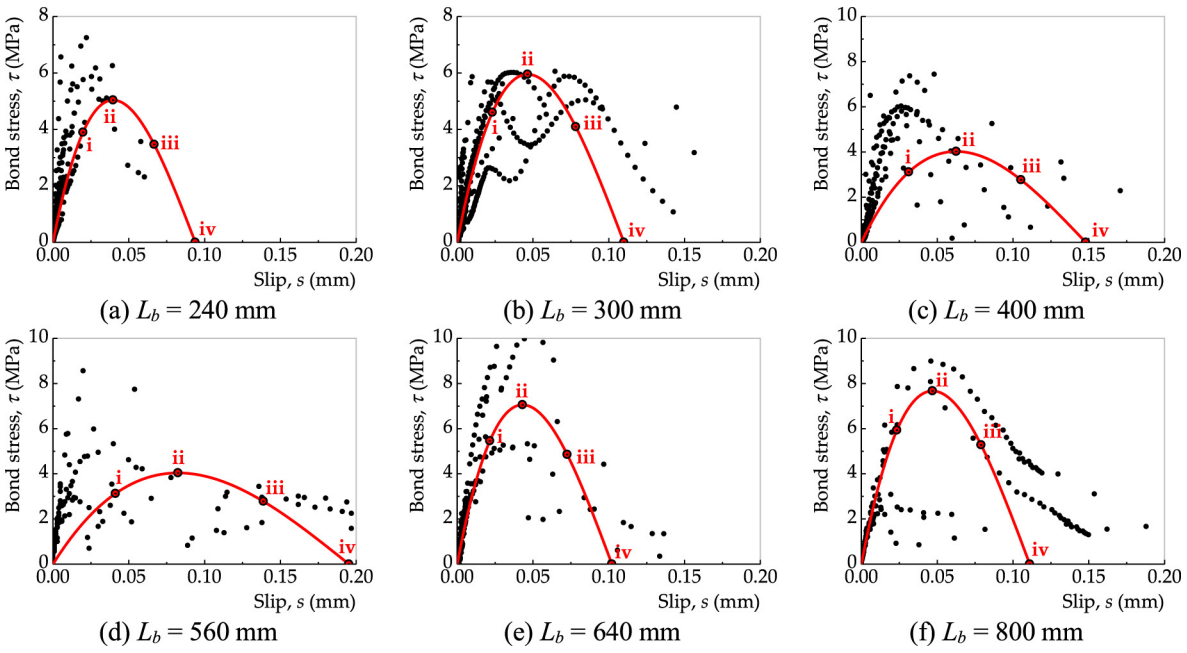


**Fig. 5 – Comparison between the proposed bond-slip model and the experimental results in [9].**

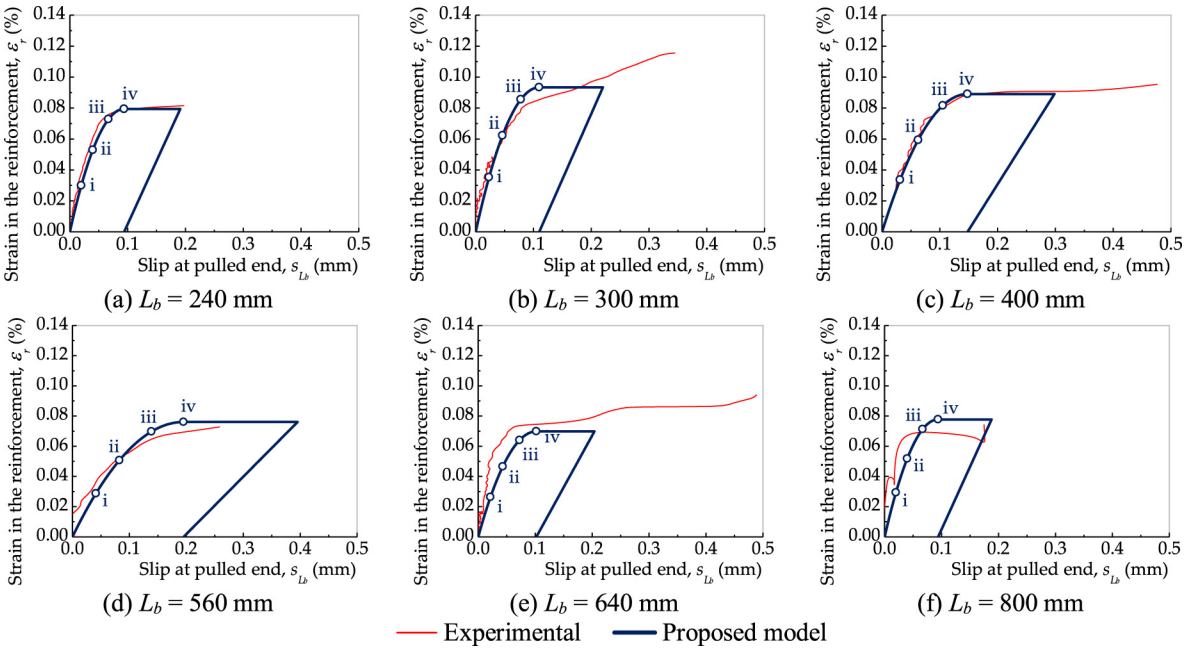


**Fig. 6 – Comparison between the theoretical strain-slip responses and those obtained from the experiments in [9].**

are shown in Fig. 7 for all six specimens. The analytical solutions for each specimen are also presented in Fig. 7 and from the comparisons between experimental and analytical results, it can be stated that, with the exceptions of specimens with $L_b$ = 300 and 400 mm, the results show good agreement. Still, it is visible that the proposed model can represent the shape of the strain distribution with higher strains developed at the pulled end and decreasing along the bond length until zero at the reinforcement free end.

### 5.3. *Bond stress distribution*

The determination of the experimental bond stresses developed within the interface of the specimens was based on

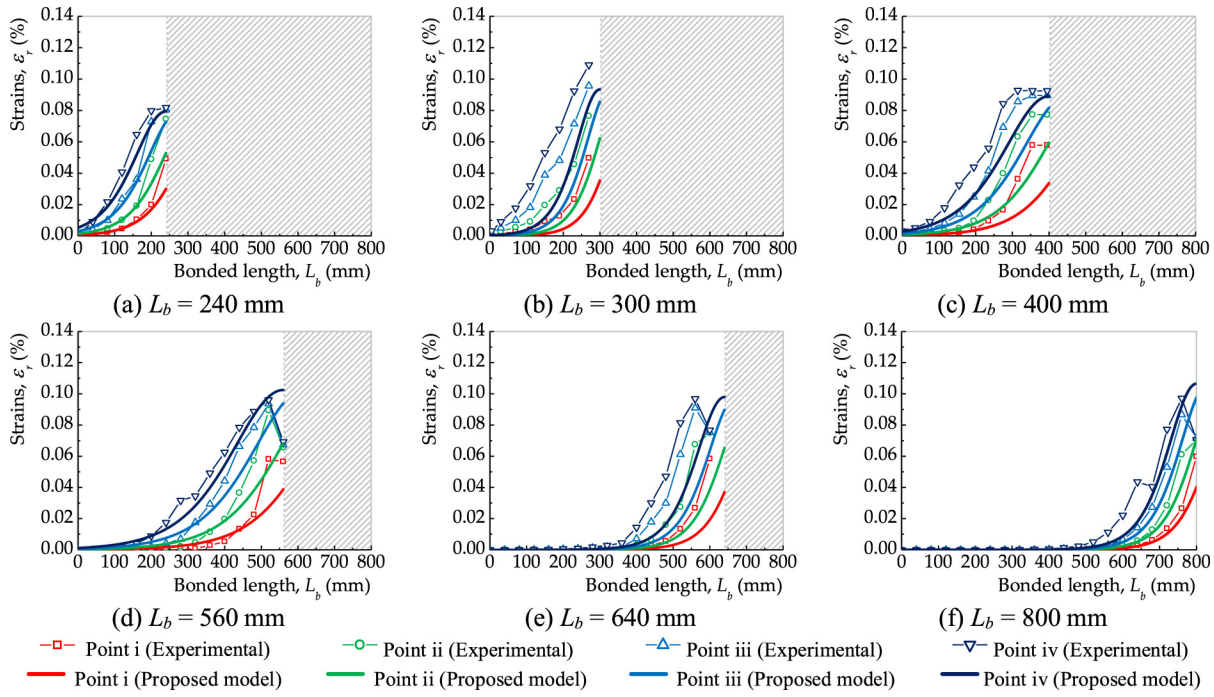


**Fig. 7 – Comparison between the theoretical strain distributions and those obtained from the experiments in [9].**

Eq. (14), which was numerically solved as follows [15,20,24,30,31,36,37]:

$$\tau\left(x_{i+1/2}\right) = E_r \cdot t_r \frac{\epsilon_{r,x_{i+1}} - \epsilon_{r,x_i}}{x_{i+1} - x_i} \tag{39}$$

where $\epsilon_{r,xi+1}$ and $\epsilon_{r,xi}$ are, respectively, the measured strains in the reinforcement at point $x_{i+1}$ and point $x_i$, i.e. from strain gauges at $x_{i+1}$ and $x_i$; and $x_{i+1} - x_i$ is the distance between two consecutive strain gauges. Fig. 8 compares the proposed closed-form solution with the experimental results obtained from the six specimens tested in [9]. From these comparisons, it can be observed that the bond stress distribution is well estimated with, perhaps, the exception of the specimens with $L_b$ = 300 and 400 mm. Nevertheless, it should be mentioned that the experimental determination of the bond slip distribution assumes that the stresses between strain gauges are constant which implies that the distance adopted between these monitoring points is important for the final results. Thus, the maximum distance adopted between consecutive strain gauges was 40 mm [9] which, in an overall overview of the results seemed to be sufficient to obtain valuable comparisons with the proposed model.

Moreover, the bond stress distributions obtained in both analytical and experimental cases correspond to what is described in the literature, i.e. with the increase of the load transmitted to the reinforcement the bond stresses increase at the pulled end until the maximum value is reached. Since maximum value is reached at the pulled end, the first stage (Elastic) of the bond-slip curve was fully used and then, the bond stresses begin to decrease according to the descending branch of the bond-slip curve usually designated as the Softening stage. In this process, the maximum bond stress moves towards the reinforcement free end. When the bond stress becomes zero at the pulled end, it means that the maximum strength of the bonded interface has been reached and the complete separation between the reinforcement and the substrate has initiated.

### 5.4. *Effective bond length*

The definition of the effective bond length ($L_{eff}$) of an adhesively bonded joint has been widely discussed in the literature, e.g. [1,13,21,38–40], and it is known that its right definition may be influenced by several parameters such as the stiffness of the reinforcement (thickness, elastic modulus), the adhesive agent (thickness, elastic modulus or resin type), substrate (elastic modulus and strength) or the surface pretreatment adopted on both materials. The ultimate slip of the interface is another parameter that has been documented in the literature as a parameter with direct impact on the effective bond length [24,27]. The fracture energy associated to the bonded interface has been considered as another parameter that may include all the others mentioned before, and when its value increases, the effective bond length decreases, as it can be seen from different expressions proposed in the literature [26,27].

The experimental tests performed in [9] allowed the determination of the relationship between the maximum loads reached in each specimen and the corresponding bonded lengths. Based on this type of graph and assuming the Rostásy and Neubauer model [14], the effective bond

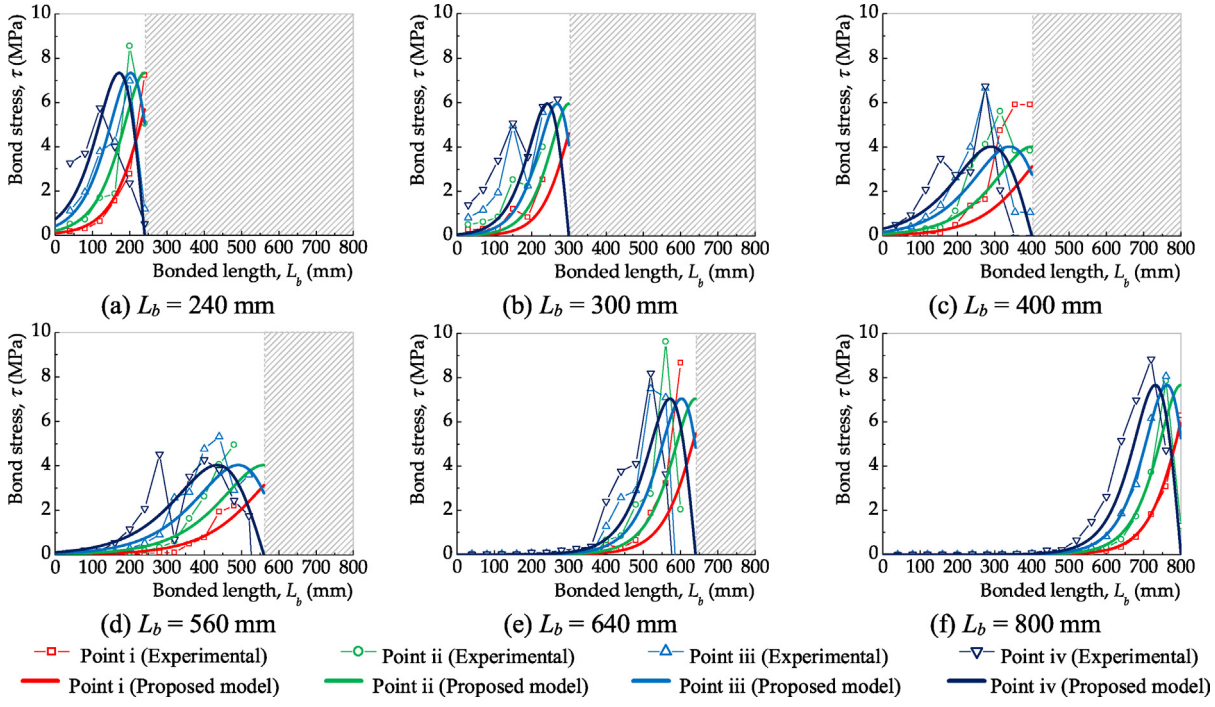


**Fig. 8 – Comparison between the theoretical bond stress distributions and those obtained from the tests in [9].**

length was determined in which the following equation was assumed if $L_b < L_{eff}$:

$$\frac{F}{F_{max}} = \frac{L_b}{L_{eff}} \cdot \left(2 - \frac{L_b}{L_{eff}}\right) \tag{40}$$

where $F$ and $F_{max}$ are the load and the maximum load transmitted to the reinforcement, respectively. Based on the experimental results, the estimation of the effective bond length was carried out through the least square minimization between the experimental and the theoretical values found for $F/F_{max}$. The equality $F/F_{max} = 1$ was adopted as a constraint in the minimization procedure if $L_b > L_{eff}$, i.e.:

$$\min_{F_{max}, L_{eff}} \sum_{j=1}^{N} \left[ \left(\frac{F}{F_{max}}\right)_{theor,j} - \left(\frac{F}{F_{max}}\right)_{exp,j} \right]^2 \tag{41}$$

where subscripts ``*theor*" and ``*exp*" denotes theoretical and experimental data, respectively, and $j$ represents the number of the test carried out until a maximum number of tests $N$. Hence, the effective bond length for the stainless steel-to-concrete interface was estimated as approximately equal to 235 mm. The estimated average value of the effective bond length through Eq. (22) is 230 mm (with a Coefficient of Variation of CoV = 11%), with the exception of specimens SS-EBR-L400 and SS-EBR-L560 which had an estimated $L_{eff}$ of 337 and 413 mm, respectively, due to the higher differences between their bond-slip curves with the remaining ones (see Fig. 4). Thus, the proposed model provides an estimation of the effective bond length that fits very well with the experimental results. This demonstrates the importance that the proposed method may have when the DIC technique is used exclusively to monitor an unknown bonded joint.

## 6. Conclusions

The proposed aim was to estimate the local bond-slip model of a joint based on the slip distribution obtained from the DIC technique. The calibration and the validation of the model were also presented and a closed-form solution to estimate the debonding process of the bonded joint subjected to a pure shear load was described. Based on the results, the following main conclusions can be drawn:

the conjunction between the use of the DIC technique and the implementation of the simplified nonlinear bond-slip model proposed in the work was proven to be a cheap and feasible solution for predicting the full-range debonding failure between a reinforcement material and a substrate;
the proposed model can be applied to a bonded joint whose local bond-slip curve is initially unknown. Unlike other cases, the proposed slip function is easy to use, and it fits very well the experimental data, which facilitates the implementation of the method for design purposes;
the proposed bond-slip curve is a 3rd degree polynomial function with three stages: Elastic, Softening and Debonded. The first Elastic stage covers all the slips smaller than $s_{max}$ and afterwards and until the $s_{ult}$ the bonded joint is subjected to the Softening stage. The Debonded stage corresponds to those slips that are higher than the ultimate slip and no bond stresses between the reinforcement and the substrate can be transferred, i.e. zero bond stress;

only two parameters are necessary to define the proposed slip function. To determine parameters $a$ and $b$, a method based on the slip distribution was proposed in which only the latter parameter is needed because the former is obtained from the curves velocity/slip vs. duration of the test. Parameter $b$ can be defined from a minimization procedure;

based on the proposed bond-slip curve, the analytical approaches for the strain distributions and bond stresses can be very useful not only due to their agreement with the experiments but also due to their simplicity, which makes them easy for practitioners, engineers and researchers to use and predict the full debonding process with feasibility;

another important parameter in the debonding between two materials is the estimation of the effective bond length which, in the present work, it is equal to 230 mm. Thus, the proposal put forward here, besides being easy to calculate, seemed to fit very well with some experimental results, leading, in comparison with the experimental campaign carried out in [9], to a relative error of only 2%.

## Acknowledgements

The first author would like to express his deepest gratitude to Fundação para a Ciência e Tecnologia for the partial financing of this work under the post-doctoral grant SFRH/BPD/111787/2015. The first and the second authors are also grateful to UNIDEMI under its Strategic Project PEst-OE/EME/UI0667/2014 and for the scientific research grant under the Strategic Project UID/EMS/00667/2013, respectively.

## REFERENCES

[1] C. Czaderski, K. Soudki, M. Motavalli, Front and side view image correlation measurements on FRP to concrete pull-off bond tests, J. Compos. Constr. 14 (4) (2010) 451–463.
[2] G. Almeida, et al., Displacement measurements with ARPS in T-Beams load tests, in: Technological Innovation for Sustainability, Springer. 349 AICT, 2011, pp. 286–293.
[3] T. Gajewski, T. Garbowski, Calibration of concrete parameters based on digital image correlation and inverse analysis, Arch. Civil Mech. Eng. 14 (1) (2014) 170–180.
[4] E. Martinelli, C. Czaderski, M. Motavalli, Modeling in-plane and out-of-plane displacement fields in pull-off tests on FRP strips, Eng. Struct. 33 (2011) 3715–3725.
[5] B. Ghiassi, et al., Application of digital image correlation in investigating the bond between FRP and masonry, Compos. Struct. 106 (2013) 340–349.
[6] H. Zhu, et al., Digital image correlation measurement of the bond-slip relationship between fiber-reinforced polymer sheets and concrete substrate, J. Reinf. Plast. Compos. 33 (17) (2014) 1590–1603.
[7] J.R. Cruz, et al., Bond behaviour of NSM CFRP-concrete systems: adhesive and CFRP cross-section influences, in: 8th International Conference on Fibre-Reinforced Polymer (FRP) Composites in Civil Engineering (CICE2016), 2016.
[8] G. Almeida, et al., In-plane displacement and strain image analysis, Comput. Aided Civil Infrastruct. Eng. 31 (4) (2016) 292–304.
[9] H.C. Biscaia, N. Franco, C. Chastre, Stainless steel bonded to concrete: an experimental assessment using the DIC technique, Int. J. Concr. Struct. Mater. 12 (2018) 9.
[10] Z. Wang, M.P. Vo, Short manual of the advanced digital image correlation function in the MOIRE Software Package, 2012, pp. 1–5. http://www.dropbox.com/s/dp7a2hspee8neak/2DDIC_manual.pdf?dl=0 (accessed October 8).
[11] http://www.ncorr.com (accessed October 8).
[12] GOM Correlate software (accessed October 8 at http://www.gom.com/3d-software/gom-correlate.html).
[13] J. Dai, T. Ueda, Y. Sato, Unified analytical approaches for determining shear bond characteristics of FRP-concrete interfaces through pullout tests, J. Adv. Concr. Technol. 4 (1) (2016) 133–145.
[14] U. Neubauer, F.S. Rostásy, Design aspects of concrete structures strengthened with externally bonded CFRP-plates, in: Proceedings of the 7th International Conference on Structural Faults and Repairs, vol. 2, 1997, 109–118.
[15] J. Dai, T. Ueda, Y. Sato, Development of the nonlinear bond stress-slip model of fiber reinforced plastics sheet-concrete interfaces with a simple method, J. Compos. Constr. 9 (1) (2005) 52–62.
[16] M. Aiello, M. Leone, Interface analysis between FRP EBR system and concrete, Compos. B: Eng. 39 (4) (2008) 618–626.
[17] H.C. Biscaia, et al., Experimental evaluation of bonding between CFRP laminates and different structural materials, J. Compos. Constr. 20 (3) (2016) 04015070.
[18] D.S. Yang, S.N. Hong, S.K. Park, Experimental observation on bondslip behavior between concrete and CFRP plate,, Int. J. Concr. Struct. Mater. 1 (1) (2007) 37–43.
[19] L. Lorenzis, B. Miller, A. Nanni, Bond of fiberreinforced polymer laminates to concrete, ACI Mater. J. 98 (3) (2001) 256–264.
[20] K. Nakaba, et al., Bond behavior between fiber-reinforced polymer laminates and concrete, ACI Struct. J. 98 (3) (2001) 359–367.
[21] H.C. Biscaia, C. Chastre, M.A.G. Silva, Nonlinear numerical analysis of the debonding failure process of FRP-to-concrete interfaces, Compos. B: Eng. 50 (2013) 210–223.
[22] W. Wu, J. Yin, Fracturing behaviors of FRP-strengthened concrete structures, Eng. Fract. Mech. 70 (2003) 1339–1355.
[23] H.C. Biscaia, C. Chastre, M.A.G. Silva, Bond-slip model for FRP-to-concrete bonded joints under external compression, Compos. B: Eng. 80 (2015) 246–259.
[24] H.C. Biscaia, et al., Numerical analysis of FRP anchorage zones with variable width, Compos. B: Eng. 67 (2014) 410–426.
[25] H.C. Biscaia, et al., Delamination process analysis of FRP-to-parent material bonded joints with and without anchorage systems using the distinct element method, Comp. Struct. 116 (2014) 104–119.
[26] E. Dehghani, et al., A new bond-slip model for adhesive in CFRP-steel composite systems, Eng. Struct. 34 (2012) 447–454.
[27] H.C. Biscaia, C. Chastre, A. Viegas, A new discrete method to model unidirectional FRP-to-parent material bonded joints subjected to mechanical loads, Comp. Struct. 121 (2015) 280–295.
[28] H. Yuan, et al., Full-range behavior of FRP-to-concrete bonded joints, Eng. Struct. 26 (2003) 553–565.
[29] J.G. Teng, H. Yuan, J.F. Chen, FRP-to-concrete interfaces between two adjacent cracks: theoretical model for debonding failure, Int. J. Solids Struct. 43 (2006) 5750–5778.
[30] H.C. Biscaia, C. Chastre, M.A.G. Silva, Linear and nonlinear analysis of bondslip models for interfaces between FRP composites and concrete, Compos. B: Eng. 45 (1) (2013) 1554–1568.
[31] B. Ferracuti, M. Savoia, C. Mazzotti, Interface law for FRP-concrete delamination, Compos. Struct. 80 (4) (2007) 523–531.
[32] H.C. Biscaia, et al., A nonlinear analytical model to predict the full-range debonding process of FRP-to-parent material

interfaces free of any mechanical anchorage devices, Compos. Struct. 138 (2016) 52–63.
[33] H.C. Biscaia, et al., Mechanical response of anchored FRP bonded joints: a nonlinear analytical approach, Mech. Adv. Mater. Struct. 25 (3) (2018) 238–252.
[34] J.F. Chen, H. Yuan, J.G. Teng, Debonding failure along a softening FRP-to-concrete interface between two adjacent cracks in concrete, Eng. Struct. 29 (2) (2007) 259–270.
[35] H.C. Biscaia, et al., Numerical modelling of the effects of elevated service temperatures on the debonding process of FRP-to-concrete bonded joints, Compos. B: Eng. 70 (2015) 64–79.
[36] H.C. Biscaia, M.A.G. Silva, C. Chastre, Factors influencing the performance of externally bonded reinforcement systems of GFRP-to-concrete interfaces, Mater. Struct. 48 (9) (2015) 2961–2981.
[37] Y. Yongming, et al., Bond characteristics of CFRP-to-steel joints, J. Constr. Steel Res. 138 (2017) 401–419.
[38] M.B. Ouezdou, A. Belarbi, S.W. Bae, Effective bond length of FRP sheets externally bonded to concrete, Int. J. Concr. Struct. Mater. 3 (2) (2009) 127–131.
[39] A. Hosseini, D. Mostofinejad, Effective bond length of FRP-to-concrete adhesively-bonded joints: Experimental evaluation of existing models, Int. J. Adhes. Adhes. 48 (2014) 150–158.
[40] H.M. Diab, O.A. Farghal, Bond strength and effective bond length of FRP sheets/plates bonded to concrete considering the type of adhesive layer, Compos. B: Eng. 58 (2014) 618–624.